Available online at www.sciencedirect.com
ScienceDirect
Geochimica et Cosmochimica Acta 72 (2008) 378–394
Geochimica et Cosmochimica Acta
www.elsevier.com/locate/gca

Continentally-derived solutes in shallow Archean seawater: Rare earth element and Nd isotope evidence in iron formation from the 2.9 Ga Pongola Supergroup, South Africa

Brian W. Alexander [a,*], Michael Bau [a], Per Andersson [b], Peter Dulski [c]

[a] *Earth and Space Sciences, Campus Ring 1, Research III 102, Jacobs University Bremen, D-28759 Bremen, Germany*
[b] *Laboratory for Isotope Geology, Swedish Museum of Natural History, SE-104 05 Stockholm, Sweden*
[c] *GeoForschungsZentrum, D-14473 Potsdam, Germany*

Received 27 November 2006; accepted in revised form 25 October 2007; available online 17 November 2007

Abstract

The chemical composition of surface water in the photic zone of the Precambrian ocean is almost exclusively known from studies of stromatolitic carbonates, while banded iron formations (IFs) have provided information on the composition of deeper waters. Here we discuss the trace element and Nd isotope geochemistry of very shallow-water IF from the Pongola Supergroup, South Africa, to gain a better understanding of solute sources to Mesoarchean shallow coastal seawater. The Pongola Supergroup formed on the stable margin of the Kaapvaal craton ~2.9 Ga ago and contains banded iron formations (IFs) that represent the oldest documented Superior-type iron formations. The IFs are near-shore, pure chemical sediments, and shale-normalized rare earth and yttrium distributions (REY_{SN}) exhibit positive La_{SN}, Gd_{SN}, and Y_{SN} anomalies, which are typical features of marine waters throughout the Archean and Proterozoic. The marine origin of these samples is further supported by super-chondritic Y/Ho ratios (average Y/Ho = 42). Relative to older Isua IFs (3.7 Ga) from Greenland, and younger Kuruman IFs (2.5 Ga) also from South Africa, the Pongola IFs are depleted in heavy rare earth elements (HREE), and appear to record variations in solute fluxes related to sea level rise and fall. Sm–Nd isotopes were used to identify potential sediment and solute sources within pongola shales and IFs. The $\epsilon_{Nd}(t)$ for Pongola shales ranges from −2.7 to −4.2, and $\epsilon_{Nd}(t)$ values for the coeval iron-formation samples (range −1.9 to −4.3) are generally indistinguishable from those of the shales, although two IF samples display $\epsilon_{Nd}(t)$ as low as −8.1 and −10.9. The similarity in Nd isotope signatures between the shale and iron-formation suggests that mantle-derived REY were not a significant Nd source within the Pongola depositional environment, though the presence of positive Eu anomalies in the IF samples indicates that high-*T* hydrothermal input did contribute to their REY signature. Isotopic mass balance calculations indicate that most (⩾72%) of the Nd in these seawater precipitates was derived from continental sources. If previous models of Fe–Nd distributions in Archean IFs are applied, then the Pongola IFs suggest that continental fluxes of Fe to Archean seawater were significantly greater than are generally considered.

1. INTRODUCTION

Studies to determine the characteristics of seawater in the geologic past are dependent upon proxies which reliably reflect seawater composition. Such studies have examined sedimentary rocks and minerals which form directly from seawater solutions, including inorganic precipitates (e.g., evaporites) or biologically mediated precipitates (e.g., $CaCO_3$). Attempts to identify reliable proxies for paleo-seawater rely on chemical tracers, particularly elements with known and predictable behavior in modern seawater and modern seawater precipitates.

* Corresponding author.
E-mail address: b.alexander@jacobs-university.de (B.W. Alexander).

0016-7037/$ - see front matter © 2007 Elsevier Ltd. All rights reserved.
doi:10.1016/j.gca.2007.10.028

These elemental tracers must also be relatively unaffected by geologic processes which commonly affect marine precipitates, such as diagenesis and metamorphism. One such group of chemical tracers are the rare earth elements and yttrium (REY), which have been used as seawater proxies in a variety of sedimentary rocks of known marine origin, including limestones, phosphorites, and banded iron formations. The usefulness of the REYs as seawater proxies has been discussed extensively by Bau and Dulski (1996), Webb and Kamber (2000), Shields and Stille (2001), Nothdurft et al. (2004), Shields and Webb (2004), and Bolhar et al. (2004). These workers have concluded that REY distributions in marine chemical sediments can accurately reflect the REY distribution of the seawater from which they formed, and that this relationship can be reliably extended to sediments from throughout the geologic record.

The information provided by the REYs regarding seawater composition is a function of the processes which control their distribution in seawater. In modern marine waters the variation in REY distributions is dominated by varying degrees of carbonate complexation, with REY principally sourced from weathering of continents, as suggested by the isotopic composition of Nd in modern seawater (Piepgras and Wasserburg, 1980). High-temperature hydrothermal inputs (e.g., black smoker fluids) are generally negligible REY sources to modern seawater, though this may not have been the case in Earth's early oceans, a scenario assessed using Eu, which is enriched in high-temperature fluids emanating from basaltic, mid-ocean ridge sources (MORB, Michard, 1989; Bau and Dulski, 1999). This approach, coupled with Nd isotope systematics, has been extended to Archean banded iron formations (e.g., Derry and Jacobsen, 1990; Danielson et al., 1992), in attempts to constrain continental- versus MORB-derived Fe inputs to Earth's early oceans (Miller and O'Nions, 1985; Jacobsen and Pimentel-Klose, 1988a). Therefore, the REY are particularly well suited not only for identifying Archean seawater proxies, but also for offering insight into the importance of mid-ocean ridge solute fluxes relative to solutes sourced from continental weathering.

Numerous workers have used Precambrian iron formations to study ancient seawater indirectly (e.g., Fryer, 1977; Jacobsen and Pimentel-Klose, 1988a; Derry and Jacobsen, 1990; Shimizu et al., 1990; Towe, 1991; Bau and Möller, 1993; among others). The similarity of REY patterns between modern seawater and both Archean iron formations and carbonates has been noted, and these chemical sediments have been used to constrain Archean seawater composition (e.g., Bau and Dulski, 1996; Kamber and Webb, 2001; Bolhar et al., 2004). Though certain features are common for many Precambrian IFs (e.g., alternating bands of Si- and Fe-rich oxide layers), variations are observed in chemical composition and mineralogy and are generally attributed to distinct differences in tectonic setting (e.g., Gross, 1983), or facies changes within a single depositional basin (Klein and Beukes, 1989). As such, Precambrian IFs formed in different marine environments may reflect potential variations in seawater composition between these environments.

Two broad types of IF are generally recognized: the *Algoma* type which is often found in greenstone belts, and the *Superior* type associated with stable sedimentary basins and cratonic margins (Gross, 1983). When considering the mass of sediment deposited, Superior-type IFs contain far more Fe than Algoma-type IFs (James and Trendall, 1982; Klemm, 2000), although this may represent a preservation bias due to their proposed tectonic settings. The association of Superior-type IFs with shelf deposits such as quartzites, carbonates, and shales is consistent with their depositional model, and Superior-type IFs are particularly useful for constraining trace element distributions in shallow Archean seawater.

The Kaapvaal craton in South Africa is widely recognized as one of the earliest stable cratons formed (Tankard et al., 1982), and hosts the oldest known Superior-type IFs in the world within the ~3.0 Ga Witwatersrand and Pongola Supergroups. Work by Beukes and Cairncross (1991) indicates that some units within both the Witwatersrand and the Pongola are correlative, however, the Pongola differs most significantly from the Witwatersrand in that it experienced lower degrees of metamorphism and structural deformation. The age, depositional environment, and the relatively pristine preservation of the Pongola Supergroup provide unique opportunities for the investigation of Archean marine chemical sediments deposited in relatively shallow waters. Rare earth and yttrium distributions and Sm–Nd isotope systematics in Pongola Supergroup IFs indicate significant continentally-derived solute fluxes to shallow Archean seawater.

2. GEOLOGIC SETTING

The 2.9–3.0 Ga Pongola Supergroup is located in eastern South Africa and southwestern Swaziland and crops out over a 270-km by 100-km area (Weilers, 1990; Fig. 1). The extent of the Pongola Supergroup is consistent with a minimum depositional area of 32,500 km^2 (Button et al., 1981), and the sequence as a whole consists of two stratigraphic units; the Nsuze Group and the overlying Mozaan Group. Sedimentary structures within Nsuze siliciclastic beds such as lenticular/flaser bedding and herringbone cross-lamination (von Brunn and Hobday, 1976) and stromatolite bearing Nsuze carbonates (Mason and von Brunn, 1977; Beukes and Lowe, 1989) indicate a near-shore shallow water depositional environment (see also Matthews, 1967; von Brunn and Mason, 1977; Tankard et al., 1982).

This study focuses on samples from the Sinqeni Formation of the Mozaan Group, which outcrops within the Wit Mfolozi inlier (Fig. 1). The Sinqeni Formation is the most laterally extensive formation within the Mozaan Group (Nhleko, 2003) and is dominated by quartz arenite and shale with minor conglomerate and banded iron formation (Matthews, 1967; Beukes and Cairncross, 1991). Specifically, the iron formation is hosted within the Ijzermijn Member, an approximately 15-m-thick unit which has shale at the base overlying with a gradational contact coarse sandstone of the older Dipka Member. The Ijzermijn shale grades upward into 3- to 5-m-thick iron formation intercalated with shale, followed again by shale which is capped

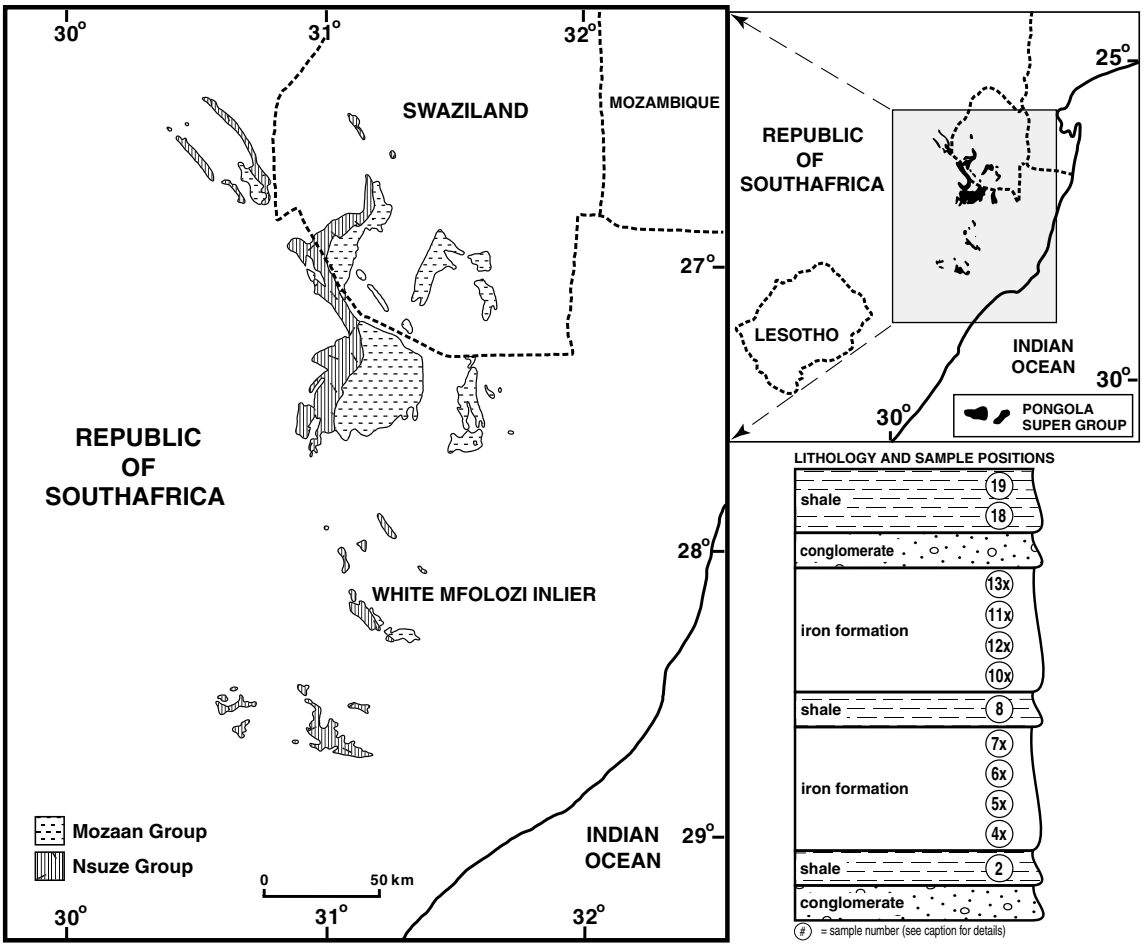

Fig. 1. Map of study area showing extent of Pongola Supergroup, location of White Mfolozi inlier, and relative positions of sampling locations within a simplified sequence stratigraphy. The *x* following some sample numbers indicates that two samples were collected, and numbered accordingly (e.g., 4*x* refers to samples 41 and 42). Thickness of the lithologic units is not to scale.

with a sharp erosional contact formed by supermature orthoquartzite (Nhleko, 2003). Sedimentary structures found within the Mozaan Group are similar to those described in the Nsuze Group, and Beukes and Cairncross (1991) recognized only two major depositional environments for the Mozaan: fluvial braidplain and shallow marine shelf systems. Studies of the Mozaan Group (Watchorn, 1980; Weilers, 1990) describe the IFs as being deposited within a distal shelf environment, conclusions that are consistent with the detailed analysis of Beukes and Cairncross (1991), who characterized the Mozaan IFs as forming on a shallow starved outer continental shelf during the peak of a marine transgression.

Age constraints for the Mozaan are not directly available from units within the group, though it appears that deposition occurred between 2940 and 2870 Ma (Beukes and Cairncross, 1991). This is inferred from a U–Pb zircon age of 2940 ± 22 Ma for rhyolite within the Nsuze Group, and a 2871 ± 30 Ma Sm–Nd mineral isochron (Hegner et al., 1984) for pyroxenite from the post-Pongola intrusive Usushwana Complex. Following deposition, the Pongola Supergroup was intruded by differentiated gabbroic sills (the Usushwana Complex), primarily along the basal unconformity and as a series of sills in the Mozaan Group (Button et al., 1981). Granitic plutons emplaced at 2.5–2.7 Ga bound the Pongola Supergroup primarily along its eastern margins, resulting in narrow contact aureoles with relatively little deformation of Pongola strata (Button et al., 1981; Tankard et al., 1982). Mineral assemblages within the Pongola generally reflect greenschist facies regional metamorphism (Tankard et al., 1982; Hegner et al., 1984; Hunter and Wilson, 1988; Beukes and Cairncross, 1991).

3. SAMPLING AND ANALYTICAL METHODS

Four shale samples and 16 iron formation samples were collected from the Sinqeni Formation in the White Mfolozi Inlier (Fig. 1). The shale and IF beds are intercalated, and are bounded at the top and bottom by beds of small pebble conglomerate. Desiccation cracks are common in the clastic units immediately above and below the sequence studied, indicating that IF deposition was preceded and followed by relatively lower seawater levels. Field sampling avoided obvious fault zones and alteration features, and fresh unweathered samples were subsequently crushed and ana-

lysed at the GeoForschungsZentrum, Potsdam, Germany. Major element concentrations were obtained by X-ray fluorescence (XRF), and mineral phase determinations were obtained by X-ray diffraction (XRD). Trace element concentrations were determined with a Perkin-Elmer/Sciex Elan Model 5000 inductively coupled plasma mass spectrometer (ICP-MS) following the procedures of Dulski (2001). Samarium and Nd concentrations were also determined using thermal ionization mass spectrometry (TIMS). Agreement between TIMS and ICPMS data is better than 2% for Nd (except shale WM2, 3.7%), and better than 4% for Sm (except shale WM2 and IF WM41, 6.1% and 6.0%, respectively). Iron-formation sample WM121 is atypical is displaying differences of 7.2% and 10.8% in respective Nd and Sm concentrations as determined by TIMS and ICPMS, yet Sm/Nd for WM121 differs by only 2.8% between the two analytical methods, and Sm/Nd comparisons between TIMS and ICPMS data never exceeds 5.3%, indicating that consistent REE ratios were determined regardless of the method used. Accuracy for other ICPMS analyses is conservatively estimated to be ±10%, and rare earth element ratios are estimated to be accurate within ±5%. Samples for Sm–Nd isotope determinations were spiked using a mixed $^{147}Sm/^{150}Nd$ spike, and processed at the Laboratory for Isotope Geology, Swedish Museum of Natural History. Samarium and Nd were separated using ion exchange techniques, and isotopic ratios were determined with a five collector Finnigan MAT 261 TIMS. Total analytical blank for Nd was approximately 40 pg, and Nd was analysed as NdO^+ in multidynamic mode, with the data being reduced assuming exponential fractionation and normalized to $^{146}Nd/^{144}Nd = 0.7219$. External precision was obtained by repeated analyses of the La Jolla standard with $^{143}Nd/^{144}Nd = 0.511853 \pm 0.000025$ (2σ, $n = 10$). Samarium was analyzed as an oxide in static mode and normalized assuming $^{149}Sm/^{152}Sm = 0.51686$. Uncertainties in TIMS determination of Sm and Nd concentrations are estimated to about <1% and 2%, respectively.

4. RESULTS

4.1. Normalization of REY and calculation of REY anomalies

In this study, normalized REY data will refer to Post Archean Average Shale (PAAS, subscript SN, McLennan, 1989), C1 chondrite (subscript CN, Anders and Grevesse, 1989), or local Archean shale (discussed below). Rare earth elements which exhibit anomalous behavior with respect to normalized data have those anomalies quantified as $[REE_X]/[REE_X^*]$, where [REE] is the measured concentration of rare earth element X, and $[REE_X^*]$ is the concentration of element X predicted by extrapolation or interpolation from adjacent REEs. Quantifying the magnitude of these anomalies in REY distributions is often complicated because adjacent REYs may themselves display anomalous behavior, as is the case with redox sensitive Ce and Eu. Normalized REY anomalies will be quantified following the methods of Bau and Dulski (1996) and Bolhar et al. (2004), and are defined as follows: $La/La^* = La/(3Pr - 2Nd)$, $Ce/Ce^* = Ce/(2Pr - Nd)$ $Eu/Eu^* = Eu/(0.67Sm + 0.33Tb)$, and $Gd/Gd^* = Gd/(0.33Sm + 0.67Tb)$.

4.2. Mozaan shales

Of the four shale samples (WM2, WM8, WM18, and WM19), three bound the bottom (WM2) and top (WM18 and WM19) of the section studied, and differ from shale WM8, which was sampled between two adjacent bands of IF and possesses distinctly different geochemical characteristics (discussed in detail below). Samples WM2, WM18, and WM19 exhibit Fe, Mn, Al, K, and Rb concentrations which compare well with published data for Mozaan shales and pelites (McLennan et al., 1983; Wronkiewicz, 1989; see Table 1). Samples WM2, WM18, and WM19 appear to represent typical clastic sediment derived from the source region for the Mozaan shales, and therefore it is appropriate to normalize data from the IF samples to the average of these three shale samples (hereafter indicated with subscript WMS). This approach of comparing Archean marine chemical sediments (IFs) to contemporaneous clastic sediment is not novel, and has been used by previous workers (e.g., Fryer, 1977; Barrett et al., 1988). While REE concentrations in the Mozaan shale average WMS are generally higher than PAAS by ~30%, the PAAS-normalized pattern of WMS is flat ($Sm/Yb = 0.97$), except for a slight enrichment in Eu, a common feature in Archean shales (Taylor and McLennan, 1985).

4.3. Mozaan iron formations

Element concentrations for 15 of the 16 iron formation samples are typical for Archean and Paleoproterozic IFs, with Si and Fe dominating the major element abundances (Table 1). The geochemistry of sample WM42 is unique in that it contains >1% Al_2O_3 and almost 15% MnO and will be discussed in detail below. Unless otherwise noted, results refer only to the remaining 15 IF samples. Normative quartz and iron-oxides combined represent 96–99% (wt.) of the samples, with Fe ranging from 10% to 81%. Aluminium, Ca, Mg, Ti, and P are present only in trace amounts, and Na and K are absent or not measurable. Other than Si and Fe, only Mn is present in appreciable amounts of the major elements studied, and averages ~1%. The mineralogy of the iron oxide component for all samples varies between magnetite and hematite, with the relative proportion of magnetite increasing with increasing Fe content. The absence of chlorite or secondary minerals indicates that the samples have experienced little alteration or weathering. Immobile trace element concentrations in the IF samples are low (<10 ppm, Table 2), consistent with the Al content of the samples.

Distributions of the REY in all samples are generally sub-parallel from the LREEs to the middle rare earth elements (MREEs). The REY distributions are not similar, however, between the middle and the heavy rare earth elements, and the patterns display two distinctly different trends (Fig. 2). Eight of the samples have relatively high $(Dy/Yb)_{WMS}$ (average 1.93) and generally higher ΣREY, whereas $(Dy/Yb)_{WMS}$ of the remaining eight samples are

Table 1
Major element data for iron formation and shales, with mineral phase determinations for IF samples

	Iron-formation samples																Shale samples[a]				
	WM41	WM42	WM51	WM52	WM61	WM62	WM71	WM72	WM101	WM102	WM111	WM112	WM121	WM122	WM131	WM132	WM2	WM8	WM18	WM19	pelite[b]
XRF (wt%)																					
SiO_2	75.4	26.2	75.7	16.8	19.7	20.7	58.8	70.8	80.9	78.4	80.3	81.0	85.8	88.0	84.4	83.6	51.6	47.9	49.1	48.6	58
Al_2O_3	0.13	1.22	0.18	0.07	0.67	0.39	0.21	0.02	0.52	0.22	nd	nd	0.06	0.06	0.34	0.10	23.3	11.9	24.7	26.8	18.8
Fe_2O_3	22.2	57.0	21.0	81.0	76.4	76.3	37.5	26.1	15.2	17.3	17.7	18.1	12.0	10.4	14.7	15.0	10.5	29.0	9.16	6.55	9.4
MnO	0.92	14.5	1.85	0.34	1.54	2.50	1.93	2.39	2.11	2.57	1.59	1.27	1.14	1.30	0.35	0.63	0.12	0.43	0.13	0.11	0.27
MgO	0.12	0.25	0.26	0.13	0.20	0.22	0.23	0.27	0.33	0.37	0.30	0.26	0.21	0.19	0.13	0.13	3.01	3.57	3.65	3.18	1.68
CaO	0.15	0.18	0.18	0.18	0.11	0.17	0.24	0.17	0.14	0.21	0.16	0.18	0.14	0.12	0.11	0.11	<0.14	0.30	<0.14	<0.14	0.08
Na_2O	nd	nd	nd	nd	nd	nd	nd	nd	nd	nd	nd	nd	nd	nd	nd	nd	0.43	<0.11	0.15	<0.11	0.28
K_2O	nd	nd	nd	nd	nd	0.01	nd	nd	0.02	0.01	nd	nd	nd	nd	nd	nd	4.07	<0.05	6.54	7.97	5.4
TiO_2	0.02	0.08	0.02	0.02	0.02	0.02	0.02	0.02	0.02	0.02	0.02	0.02	0.02	0.02	0.02	0.02	0.90	0.72	1.35	1.21	0.82
P_2O_5	0.02	0.08	0.03	0.05	0.05	0.05	0.02	0.02	0.04	0.04	0.03	0.03	0.03	0.02	0.02	0.03	0.07	0.05	0.08	0.04	0.09
LOI	nd	nd	nd	nd	nd	nd	nd	nd	nd	nd	nd	nd	nd	nd	nd	nd	5.01	5.17	5.15	4.96	4.5
Total	98.96	99.51	99.22	98.59	98.69	100.36	98.95	99.79	99.28	99.14	100.10	100.86	99.40	100.11	100.07	99.62	99.01	99.04	100.01	99.42	99.32
XRD (wt%)																					
Quartz	87.0	85.0	88.0	37.0	39.0	39.0	80.0	92.0	94.0	94.0	92.0	91.0	95.0	96.0	87.0	88.0					
Magnetite	Trace	Trace	7.0	46.0	39.0	38.0	9.0	3.0	3.0	3.0	5.0	7.0	2.0	1.0	nd	nd					
Hematite	13.0	15.0	5.0	17.0	22.0	22.0	12.0	5.0	3.0	4.0	4.0	2.0	4.0	3.0	13.0	12.0					
Chlorite	nd	nd	nd	nd	nd	nd	nd	nd	nd	nd	nd	nd	nd	nd	nd	nd					

nd, not detected.

[a] Average of shale samples WM2, WM18, and WM19 used as representative Mozaan shale (WMS).

[b] Average of 15 pelite samples from Mozaan Group (data from Wronkiewicz, 1989).

Table 2
Trace element concentrations in iron-formation and shale samples (mg/kg)

	Iron-formation samples																Shale samples				
	WM41	WM42	WM51	WM52	WM61	WM62	WM71	WM72	WM101	WM102	WM111	WM112	WM121	WM122	WM131	WM132	WM2	WM8	WM18	WM19	pelite[a]
Rb	<0.5	4.9	<0.5	<0.5	1.0	1.5	<0.5	<0.5	2.2	1.2	<0.5	<0.5	<0.5	<0.5	<0.5	<0.5	125	0.98	236	263	*235*
Sr	1.9	139	25.5	6.3	10.4	20.2	13.8	13.1	20.8	34.2	20.6	19.8	8.8	7.6	7.9	13.8	49.4	7.6	16.3	13.0	*28*
Y	1.35	10.5	1.15	2.51	3.43	3.61	1.12	1.11	1.66	1.56	1.22	1.12	0.73	0.72	1.22	4.82	40.4	10.3	29.2	19.3	*36*
Zr	<1	29.0	<1	1.3	1.5	2.1	1.7	1.3	<1	<1	<1	<1	<1	<1	<1	<1	208	145	239	207	*270*
Cs	0.189	0.513	0.084	0.063	0.069	0.085	0.035	0.027	0.118	0.142	0.396	0.425	0.127	0.118	0.282	0.318	3.24	0.146	5.84	8.05	9.3
Ba	<2	14.3	5.4	3.2	10.6	49.5	11.8	13.1	42.5	34.4	14.4	6.1	2.5	2.1	13.7	23.8	331	39.4	919	991	510
La	0.538	7.12	0.482	1.73	2.33	2.27	1.01	0.706	0.897	0.971	0.625	0.531	0.370	0.298	0.631	0.782	34.3	17.6	95.2	42.3	38
Ce	1.08	12.9	0.905	3.01	4.04	3.93	1.63	1.19	1.65	1.47	1.13	0.988	0.509	0.415	1.24	1.21	67.9	27.9	181	82.5	80
Pr	0.134	1.58	0.118	0.385	0.481	0.486	0.185	0.138	0.190	0.179	0.148	0.129	0.055	0.044	0.173	0.195	8.30	2.69	19.4	9.48	—
Nd	0.524	6.25	0.466	1.47	1.76	1.79	0.672	0.538	0.762	0.670	0.550	0.502	0.208	0.175	0.762	0.884	29.6	8.08	65.5	34.2	—
Sm	0.157	1.46	0.111	0.321	0.375	0.366	0.121	0.108	0.169	0.141	0.122	0.111	0.041	0.036	0.221	0.278	5.96	1.35	9.62	5.87	6.2
Eu	0.066	0.567	0.052	0.139	0.141	0.139	0.042	0.038	0.061	0.054	0.047	0.044	0.017	0.018	0.088	0.129	1.36	0.320	1.96	1.09	1.42
Gd	0.227	2.05	0.142	0.394	0.457	0.476	0.134	0.128	0.215	0.188	0.160	0.146	0.059	0.058	0.273	0.524	7.22	1.23	6.12	3.91	—
Tb	0.038	0.277	0.023	0.059	0.073	0.075	0.021	0.018	0.033	0.026	0.021	0.020	0.007	0.007	0.037	0.089	1.24	0.201	0.96	0.60	0.89
Dy	0.223	1.54	0.141	0.350	0.459	0.463	0.128	0.120	0.219	0.178	0.130	0.117	0.052	0.049	0.204	0.574	7.82	1.29	5.63	3.79	—
Ho	0.043	0.294	0.031	0.067	0.092	0.095	0.028	0.026	0.047	0.040	0.026	0.026	0.012	0.011	0.035	0.121	1.55	0.304	1.17	0.783	—
Er	0.116	0.785	0.086	0.170	0.238	0.257	0.085	0.083	0.143	0.118	0.077	0.075	0.038	0.039	0.085	0.317	4.45	1.04	3.62	2.58	—
Tm	0.015	0.104	0.012	0.021	0.029	0.031	0.012	0.012	0.021	0.018	0.011	0.010	0.005	0.005	0.010	0.037	0.651	0.159	0.58	0.39	—
Yb	0.082	0.596	0.070	0.097	0.154	0.165	0.077	0.076	0.148	0.111	0.060	0.057	0.029	0.031	0.051	0.188	4.19	1.16	4.27	2.76	3.4
Lu	0.011	0.091	0.010	0.013	0.022	0.025	0.012	0.012	0.022	0.019	0.010	0.009	0.005	0.005	0.007	0.026	0.599	0.182	0.65	0.46	0.54
Hf	<0.05	0.75	<0.05	<0.05	<0.05	<0.05	<0.05	<0.05	<0.05	<0.05	<0.05	<0.05	<0.05	<0.05	<0.05	<0.05	5.68	3.85	6.12	5.34	8.4
Pb	1.42	9.23	1.14	1.06	0.86	0.96	0.87	0.89	1.14	2.33	3.67	3.54	1.54	1.38	4.04	4.75	3.43	2.38	3.8	1.90	*13*
Th	<0.05	0.78	<0.05	0.06	0.07	0.08	0.07	0.06	0.07	0.05	<0.05	<0.05	<0.05	<0.05	<0.05	<0.05	10.5	6.39	16.3	10.2	8.6
U	0.55	1.95	0.06	0.15	0.08	0.10	0.08	0.05	0.09	0.11	0.03	0.03	0.02	0.02	0.25	0.36	1.58	0.916	5.24	2.68	2.3
ΣREY	4.6	46	3.8	10.7	14.1	14.2	5.3	4.3	6.2	5.7	4.3	3.9	2.1	1.9	5.0	10.2	216	74	425	210	—
$(La/La^*)_{WMS}$[b]	1.16	1.34	1.21	1.21	1.17	1.15	1.3	1.46	1.47	1.39	1.06	1.17	1.76	2.06	1.69	2.21	0.94	1.11	1.00	1.04	
$(Gd/Gd^*)_{WMS}$[b]	1.15	1.34	1.15	1.20	1.14	1.17	1.13	1.25	1.19	1.30	1.35	1.31	1.49	1.51	1.30	1.19	1.08	1.04	0.94	0.97	
$(Eu/Eu^*)_{CN}$[b]	1.11	1.10	1.30	1.24	1.06	1.05	1.01	1.03	1.02	1.10	1.12	1.14	1.21	1.41	1.17	1.10	0.63	0.72	0.67	0.60	0.70

[a] Data from Wronkiewicz (1989) and equals the average of 15 pelite samples from Mozaan Group, where all concentrations determined by INAA, except italicized data which were determined by XRF.

[b] Subscript for calculated La/La^*, Gd/Gd^*, and Eu/Eu^* refers to data normalized either to average of Mozaan shale samples WM2, WM18, and WM19 (WMS) or chondrite (CN). See text for details.

considerably lower (average 1.13). The REY patterns are not correlated with major element chemistry, nor with immobile trace element content, but the two groups of patterns can be distinguished on the basis of relative stratigraphic position; i.e., high $(Dy/Yb)_{WMS}$ corresponds to samples collected at the base and at the top of the sequence studied, and low $(Dy/Yb)_{WMS}$ is found in samples collected from the middle of the sequence.

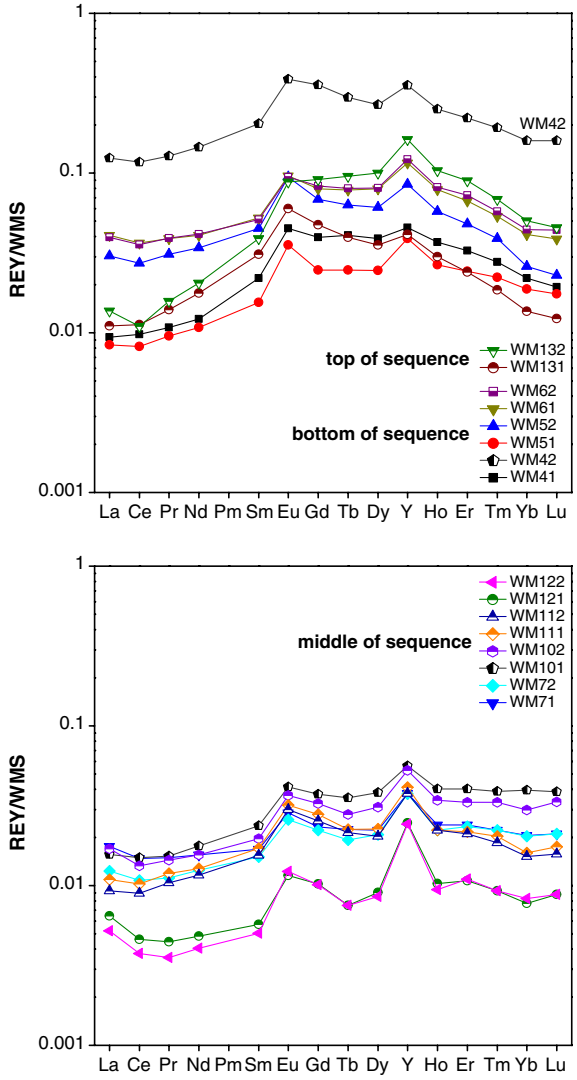

Fig. 2. REY distributions in iron-formation samples normalized to Mozaan shale average WMS to facilitate comparison with contemporaneous continental crust. Samples generally exhibit positive La, Gd, and Eu anomalies which are characteristic of marine chemical sediments regardless of age. All samples display generally parallel patterns from the light- to middle-rare-earth elements. From the MREE to the HREE, the patterns are not parallel, and two groups of patterns can be distinguished. Samples from the bottom and top of the sequence (top figure) have relatively higher REY concentrations, smaller Y anomalies, and decrease from the MREE to the HREE, compared to samples obtained from the middle of the sequence studied (bottom figure). The REY patterns track a full transgressive–regressive cycle, and variations in these patterns mirror inferred water depths based on lithology (i.e., transition from deposition of conglomerate to IF and back to conglomerate deposition).

The REY patterns of all the IF samples exhibit WMS-normalized positive La, Eu, and Gd anomalies. Calculated $(La/La^*)_{WMS}$ and $(Gd/Gd^*)_{WMS}$ are above unity for all 16 IF samples (Fig. 3), and $(Eu/Eu^*)_{WMS}$ ranges from 1.51 to 2.09 (average 1.69). The magnitude of the La, Eu, and Gd anomalies are indistinguishable on the basis of stratigraphic position. Y/Ho averages 42 for all samples, and higher Y/Ho values are observed for samples collected from the middle of the sequence, though the difference between the two groups is small when samples WM121 and WM122 (Y/Ho of 61 and 66, respectively) are not considered.

The REY pattern of sample WM42 is similar to samples obtained stratigraphically above and below it, possessing positive La, Gd, and Y anomalies. The ΣREY content is the highest of the IF samples, and though most major element concentrations for sample WM42 are comparable to the other IF samples, Al_2O_3 is enriched at 1.2% and MnO is significantly higher (14.5%). WM42 also contains somewhat greater concentrations of Rb, and significantly more Zr, Hf and Th than any of the other 15 IF samples.

Seven iron-formation samples and three shale samples were analyzed using TIMS, and Nd and Sm isotope data are presented in Table 3. Six of the samples (one shale and five IF samples) display similar $^{147}Sm/^{144}Nd$ between 0.1164 and 0.1486, values common to other Archean shales and iron formation (e.g., Miller and O'Nions, 1985; Alibert and McCulloch, 1993; Jahn and Condie, 1995; Bau et al., 1997). Of the remaining four samples, two are iron formations displaying the highest $^{147}Sm/^{144}Nd$ observed (>0.17), whereas the lowest $^{147}Sm/^{144}Nd$ values are observed in the remaining two shale samples (<0.10). The isotopic behavior of Nd is expressed using $\epsilon_{Nd}(t)$ (DePaolo and Wasserburg, 1976), which reflects the relative difference between

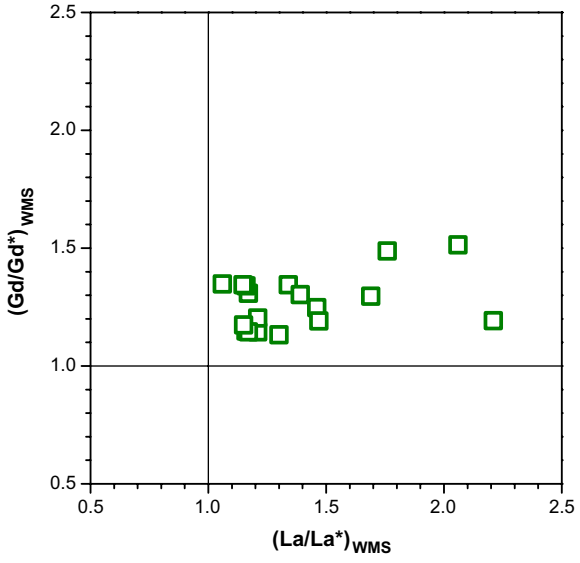

Fig. 3. La and Gd anomalies of iron formation samples normalized to WMS. All samples display La/La* and Gd/Gd* above unity, features characteristic of marine chemical sediments.

Table 3
Nd and Sm concentrations (mg/kg) and isotopic data determined by TIMS for 2.9 Ga Mozaan shales and iron-formations

Sample	Nd (ppm)	Sm (ppm)	$^{143}Nd/^{144}Nd \pm 2\sigma$[a]	$^{147}Sm/^{144}Nd \pm 2\sigma$	$\epsilon_{Nd}(0)$	$\epsilon_{Nd}(2.9\ Ga)$
Shale						
WM2	30.7	6.34	0.511120 ± 25	0.1247 ± 6	−29.61	-2.7 ± 0.3
WM8	8.19	1.33	0.510543 ± 25	0.0979 ± 5	−40.87	-4.0 ± 0.6
WM18	64.7	9.70	0.510389 ± 25	0.0905 ± 5	−43.87	-4.2 ± 0.3
Iron formation						
WM41	0.520	0.148	0.511754 ± 25	0.1721 ± 9	−17.24	-8.1 ± 0.7
WM51	0.457	0.112	0.511587 ± 25	0.1486 ± 7	−20.50	-2.6 ± 0.8
WM61	1.76	0.362	0.511029 ± 25	0.1242 ± 6	−31.39	-4.3 ± 0.6
WM72	0.533	0.104	0.511203 ± 25	0.1302 ± 7	−27.99	-3.2 ± 0.6
WM102	0.659	0.146	0.511322 ± 25	0.1330 ± 7	−25.67	-1.9 ± 0.7
WM121	0.194	0.037	0.510921 ± 25	0.1164 ± 6	−33.49	-3.5 ± 0.5
WM131	0.762	0.215	0.511698 ± 25	0.1766 ± 9	−18.34	-10.9 ± 0.6
WM131r[b]	0.748	0.218	0.511734 ± 25	0.1763 ± 9	−17.63	-10.1 ± 0.8
BCR-2 (3 mg)	28.8	6.6	0.512619 ± 25	0.1378 ± 7		

[a] The errors in the $^{143}Nd/^{144}Nd$ refer to the last digits and are estimated from repeated analysis of the La Jolla standard which gave $^{143}Nd/^{144}Nd = 0.511853 \pm 0.000025$ (2σ, $n = 10$).
[b] Replicate digestion, column separation, and analysis of sample WM131.

$^{143}Nd/^{144}Nd$ of the sample, and $^{143}Nd/^{144}Nd$ within a chondritic uniform reservoir (CHUR) at any given time t. For the shale samples, $\epsilon_{Nd}(t)$ falls within a narrow range from −2.74 to −4.24, whereas the IF samples display a bimodal $\epsilon_{Nd}(t)$ distribution, with most samples exhibiting $\epsilon_{Nd}(t)$ similar to the shales, while the two IF samples with $^{147}Sm/^{144}Nd > 0.17$ (WM41 and WM131) have significantly more negative $\epsilon_{Nd}(t)$ values of −8.1 and −10.9, respectively.

5. DISCUSSION

5.1. Depositional controls on REYs in Mozaan IFs

The Mozaan IFs REY distributions might have been affected by a number of processes including: (i) post- and syn-depositional processes, (ii) the degree to which the REY were scavenged by particulate matter in the water column prior to deposition, and (iii) also by the various inputs to the seawater from which the IFs precipitated.

Potential post-depositional mechanisms affecting trace metal and REY distribution in the Mozaan IFs include diagenetic and metamorphic processes. During diagenesis, mobility of the REY would tend to average out REY distributions in banded iron formations, yet Bau and Dulski (1992) observed highly variable REY ratios in individual Fe- and quartz-rich bands within the 2.46 Ga Superior-type Kuruman IF. Such variation is also present in REY data for IF mesobands from the Dales Gorge Member in the Hamersley Group of Australia (Morris, 1993). Bau (1993) studied the impact of post-burial processes on REY signatures in Precambrian IFs from the Hamersley Basin in Western Australia, the Kuruman and Penge IFs in South Africa, and the Broomstock IFs of Zimbabwe, and concluded that REYs are effectively immobile during diagenesis and lithification.

The effects of metamorphism on REY mobility is a function of water/rock ratios, with LREE depletion and negative Eu anomalies expected in rocks that host significant amounts of metasomatic fluids during metamorphism (Grauch, 1989; Bau, 1993). Iron-formation samples from regions that have experienced high grade metamorphism (e.g., Isua, Greenland) do not exhibit Eu or LREE depletion, and in general coeval detritus free IF samples display similar REY_{CN} patterns regardless of metamorphic grade (Bau, 1991, 1993). Therefore, the relatively low-grade greenschist facies metamorphism which affected Mozaan IF samples would not have had a significant effect on their REY distribution.

For syn-depositional processes, REY patterns in chemical precipitates may be fractionated with respect to contemporaneous seawater due to the presence of detrital aluminosilicates, or as a result of exchange effects between REY scavenging particulates and marine waters. The effect of clastic contamination can be assessed using trace elements that are essentially immobile in aqueous solutions, and hence occur only at ultra-trace levels in seawater. The low abundances in the Mozaan IFs of such elements as Al, Ti, Zr, Hf, Y, and Th demonstrates that these are very pure chemical sediments and that clastic contamination is negligible, which is consistent with a sediment-starved continental shelf depositional environment for the Mozaan IFs (e.g., Beukes and Cairncross, 1991).

The influence of solution complexation, fractionation, and scavenging within the marine environment on REY distributions in IFs is more difficult to assess. The REY concentration in modern seawater is controlled primarily by scavenging particulate matter (e.g., Elderfield, 1988; Erel and Stolper, 1993), to the extent that seawater abundances of REYs are extremely low. The association between Fe-rich colloids and REYs has led many workers to conclude that Fe-oxyhydroxide particles dominated REY scavenging during the formation of ancient metalliferous sediments (e.g., Derry and Jacobsen, 1990). This scavenging should represent the balance between two competing effects; the solution complexation of the REYs and the Fe-oxyhydroxide surface complexation. This model assumes that the reac-

tion kinetics of adsorption/desorption are significantly faster than the particle residence time in an oxic water column. This assumption is supported by experimental evidence indicating that particle-surface/solution REY exchange equilibrium occurs within minutes (Bau, 1999), suggesting that most Fe-oxyhydroxide particles settling through an oxic water column (of relatively constant REY distribution) should be in equilibrium with the solution phase.

Natural systems that provide insight into such equilibrium exchange processes are available in the form of modern marine hydrogenetic ferromanganese crusts and terrestrial spring-water precipitates. Seafloor Fe–Mn crusts have trace metal distributions that reflect equilibrium adsorption–desorption processes between REYs and seawater, processes that strongly fractionate REYs. Very similar fractionation is observed between Fe-oxyhydroxides and terrestrial spring water (Bau et al., 1998). The most striking difference between these precipitates and the respective fluids which formed them is the lower Y/Ho observed in the precipitates, which display negative Y anomalies. This Y–Ho fractionation is due to the preferential sorption of Ho relative to Y on the scavenging Fe(–Mn) particles (e.g., Bau et al., 1996, 1998). Preferential adsorption of Ho over Y on Fe-oxyhydroxides has been demonstrated experimentally (Bau, 1999) and is completely consistent with the observed fractionation of Y and Ho during precipitation of hydrogenetic Fe–Mn crusts from seawater. We emphasize that such Y–Ho fractionation is not observed in Archean iron formations.

If redox conditions in Archean seawater permitted the precipitation of ferric iron, and if scavenging Fe-oxyhydroxide particles achieved exchange equilibrium with surrounding seawater, the above observations predict subchondritic values of Y/Ho in the IFs. The significantly higher Y/Ho observed in IFs of different ages strongly suggests that Fe-oxyhydroxide particles that scavenged REYs could not be at or near exchange equilibria with respect to ambient seawater (Bau and Dulski, 1996). Although the actual reason why IFs display the REY seawater pattern has not been satisfactorily explained and requires further investigation, the striking similarity between REY patterns in Archean marine carbonates and IFs suggests that pure Archean IFs faithfully record the REY distributions of contemporaneous seawater.

5.2. Archean seawater

5.2.1. High-temperature hydrothermal input

The geologic setting and low detritus content, coupled with the observed LREE depletions and positive La, Gd, and Y anomalies (Figs. 2 and 5), strongly suggests the Mozaan IFs represent ~3.0 Ga seawater. Working under the assumption that these sediments possess trace element distributions reflective of contemporaneous seawater, some general constraints may be placed on the composition of Archean seawater.

The occurrence of the oxide-facies Mozaan IFs suggests that the redox level of even very shallow seawater permitted nearly continuous precipitation of significant amounts of Fe(III)-bearing (hydr)oxides, while the lack of any Ce anomaly in normalized data indicates that no process operated during Fe-sedimentation that was capable of fractionating Ce. This scenario is clearly different from the oxic modern marine system, in which Ce is oxidized to immobile Ce(IV) on particle surfaces, resulting in fractionation from the other REY and producing the strong negative Ce anomaly observed in modern seawater. The lack of significant negative-Ce anomalies in many Archean chemical sediments has been discussed by numerous authors in terms of the oxidation history of the Earth's surface (e.g., Fryer, 1977; Derry and Jacobsen, 1990; Kato et al., 1998; among others). While the exact process that converted large amounts of Fe(II) to Fe(III) in seawater during sedimentation of the Mozaan IFs is unknown, the Ce distributions in these chemical precipitates indicate Archean seawater did not possess a negative Ce anomaly, and correspondingly, redox levels were lower than those observed in modern marine systems.

Unlike Ce, the Mozaan IFs display pronounced positive Eu anomalies (Fig. 4), which in modern marine environments are only observed in high-temperature (>250 °C) hydrothermal fluids, such as those typically found at mid-ocean ridges and back-arc spreading centers. It is reasonable that the REY_{CN} patterns of these high-T fluids in the Early Precambrian were similar to those observed today and exhibited Eu anomalies >1 and enrichment in LREEs (Bau and Möller, 1993), features which are characteristic

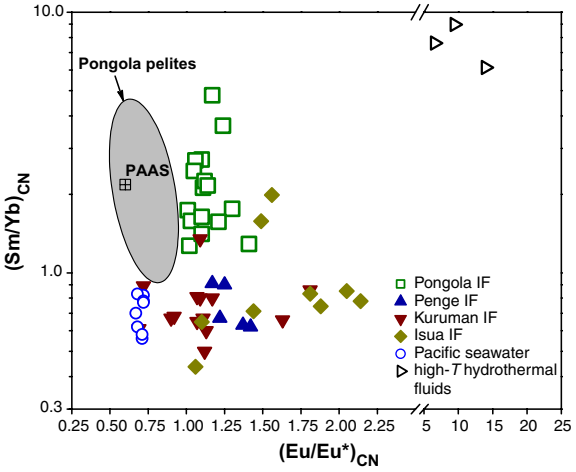

Fig. 4. Plot of chondrite-normalized Sm/Yb and Eu/Eu* for Mozaan IFs, and including data for 3.7 Ga Isua IFs (Bolhar et al., 2004), 2.5 Ga Kuruman and Penge IFs (Bau and Dulski, 1996), shallow (<500 m) Pacific seawater (Alibo and Nozaki, 1999), and high-T hydrothermal fluids (>350 °C, Bau and Dulski, 1999). Note break in horizontal axis. Isua samples are those considered by Bolhar et al. (2004) to reflect contemporaneous seawater. The grey shaded area represents the range of values for 62 pelites from the Pongola Supergroup sampled by Wronkiewicz (1989), and the crossed-square represents Post-Archean Average Shale (PAAS, McLennan, 1989). The Mozaan IFs exhibit Eu/Eu* between that of the Isua and Kuruman IFs, yet display Sm/Yb values similar to continental crust and significantly higher than any of the other IFs (except for two Isua and one Kuruman sample). All IF samples have significantly lower Sm/Yb and Eu/Eu* than high-T hydrothermal fluids.

of the Mozaan IF samples (Fig. 4). The presence of positive Eu anomalies is clear evidence that REY from high-*T* hydrothermal inputs influenced the continental shelf environment that hosted the Mozaan IFs.

For constraints on ancient hydrothermal fluxes, modern black smoker fluids offer the best analogs for the trace element compositions of high-*T* fluids which contributed to the REY distribution in Archean iron formations. For the Mozaan IFs, the magnitude of the positive Eu anomalies generally compare well with data for other IFs (Fig. 5). However, the general REY distributions of the Mozaan IFs are significantly different when compared to well studied examples such as the 3.7 Ga Isua IF of Greenland (Bolhar et al., 2004) and the 2.5 Ga Kuruman IF from South Africa (Bau and Dulski, 1996), though regardless of age, these iron formations display the seawater characteristics of marine chemical sediments (Fig. 5). Conservative mixing calculations indicate that a high-*T* hydrothermal fluid contribution of less than 0.1% is adequate for producing the Eu/Sm ratios observed within the Pongola and Kuruman IFs, and reasonably accounts for most of the Eu/Sm ratios observed in the Isua IFs

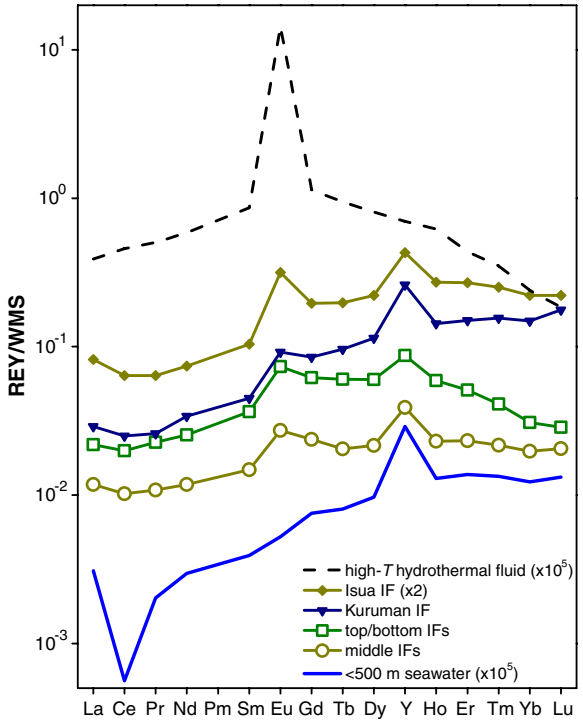

Fig. 5. REY distributions of average Mozaan, Isua, and Kuruman IFs, as well as average high-*T* hydrothermal fluid and average shallow (<500 m) Pacific seawater (see Fig. 4 caption for data sources). Mozaan data represent averages of the two distinct groups of REY patterns shown in Fig. 2: *top/bottom* is the average of seven samples from the top and bottom of the sequence studied (excluding sample WM42), and *middle* refers to the eight IF samples from the middle of the sequence. All of the IFs show positive shale-normalized La, Gd, and Y anomalies typical of seawater and a general enrichment of HREEs over LREEs. Note the generally flat pattern of the Mozaan IF averages from Sm to Yb compared to the other Archean iron formation.

(Fig. 6a). This is comparable with the model of Klein and Beukes (1989), who noted that a 1000:1 mixing ratio of typical North Atlantic seawater with deep sea hydrothermal fluids produced REY patterns similar to that of numerous Precambrian IFs. An identical seawater/hydrothermal fluid mixing ratio of 1000:1 was also calculated by Khan et al. (1996) as sufficient to account for the REY distributions in IFs from the 2.6–3.0 Ga Kushtagi schist belt. Therefore, it appears that relatively minor inputs (<1%) of high-*T* hydrothermal fluids during conservative mixing may reasonably account for Eu/Sm observed within a wide variety of Archean IFs.

The differences between the REY distribution of the Mozaan IFs relative to other IFs does suggest a greater input of 'Archean black smoker' fluids, particularly with respect to Sm/Yb. These fluids possess higher Sm/Yb and chondritic Y/Ho values (~28) when compared to modern seawater, and these ratios provide additional constraints on the mixing model (Fig. 6b). Mixing calculations indicate that a 1–5% contribution of hydrothermal fluids may account for the Y/Ho and Sm/Yb observed within the Mozaan IFs. However, this mixing ratio is inconsistent with the 0.1% contribution of high-*T* fluids necessary to account for Eu/Sm (Fig. 6c). It is worth noting that all of the Mozaan samples, regardless of stratigraphic position, exhibit Sm/Yb higher than average Kuruman or Isua IFs (0.68 and 0.86, respectively). Except for two Isua samples and one Kuruman sample, the general HREE depletion exhibited within the Mozaan IFs is not observed in the older or younger iron formations. The poor fit of the mixing model in explaining the relatively high Sm/Yb of the Mozaan IFs suggests different processes controlled the REY distributions in the Kuruman and Isua IFs and indicates the possible existence of additional REY sources to the Mozaan samples.

5.2.2. *Low-temperature fluid input*

In addition to the high-*T* component expected in deep Archean seawater, the marine bottom water component would be influenced by low-*T* solutions (<200 °C) altering oceanic crust and fluxes from porewaters sourced from sediments. Wheat et al. (2002) examined <100 °C hydrothermal fluids venting from the flank of the Juan de Fuca ridge and did not observe either a significant enrichment in Eu or a significant fractionation of Sm/Yb in the low-*T* fluid endmember relative to seawater. Trace element data for near-shore, low-*T* (≤100 °C) hydrothermal vent fluids (Pichler et al., 1999) suggests REY distributions similar to seawater and negligible Eu enrichment compared to host rocks. Therefore, compared to high-*T* fluids, low-*T* hydrothermal fluids would likely exhibit no positive Eu_{CN} anomaly and lower $(Sm/Yb)_{CN}$. Therefore, even though the Mozaan IFs formed in a shallow near-shore depositional environment, the positive Eu anomalies observed indicate that high-*T* hydrothermal inputs were one REY source for the Mozaan IFs. Whereas constraints can be placed on the relative contribution of these high-*T* hydrothermal fluids in an effort to explain Sm/Yb and Eu/Sm within the Mozaan IF, this is not possible for the low-*T* component. In a reducing Archean ocean deep water benthic

fluxes of trace elements would be expected to affect the REY distribution of the bottom water component, and though such fluxes are at best difficult to characterize, it can be ruled out that such low-*T* input would have displayed positive Eu anomalies.

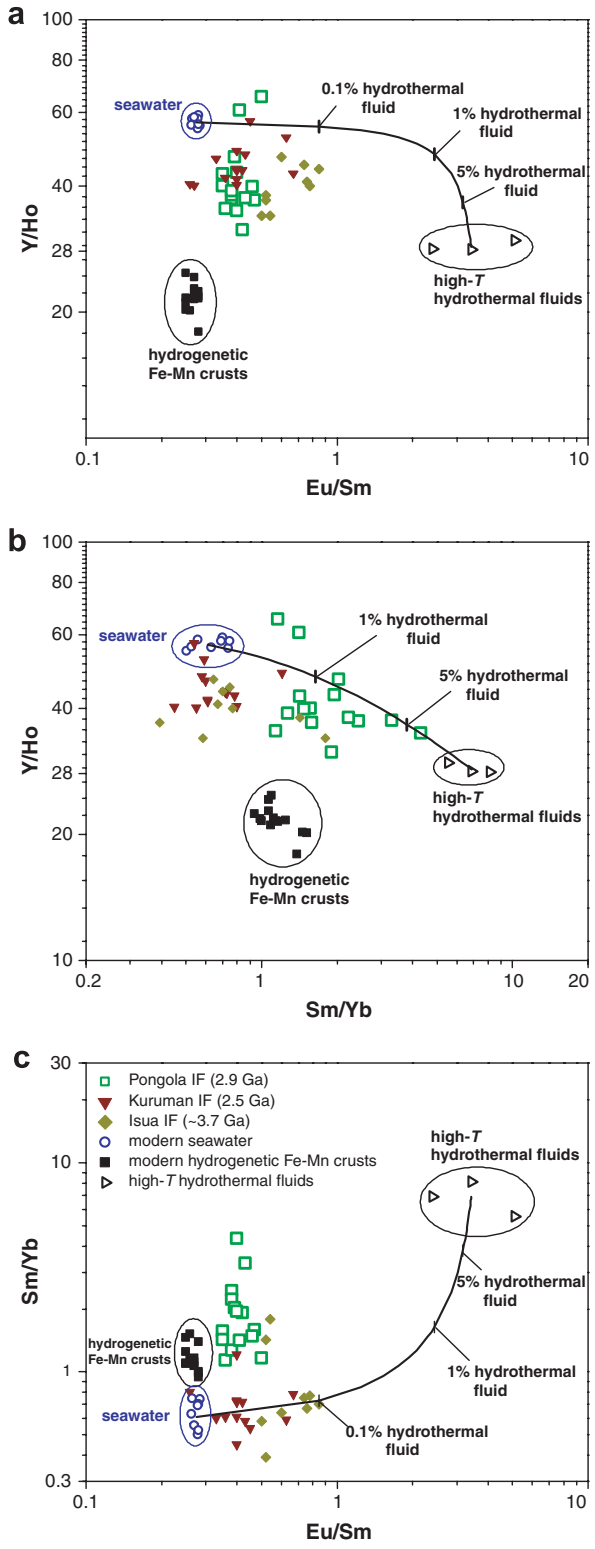

5.2.3. Surface seawater input

The major remaining REY input affecting the Mozaan IFs would be Archean surface seawater. Rare earth element distributions in modern seawater, while exhibiting local variability and distinct trends with depth, are generally consistent with the pattern shown in Fig. 5, and exhibit a $(Sm/Yb)_{CN}$ ratio of ~0.8. A study by Elderfield et al. (1990) reported REY data for five coastal seas (salinity > 20‰) that exhibited $(Sm/Yb)_{CN}$ ranging from 0.70 to 1.24, consistent with coastal seawater from the East Frisian islands (North Sea) that displays $(Sm/Yb)_{CN}$ between 0.61 and 0.73 (Kulaksiz and Bau, 2007). Elderfield et al., 1990 also presented REY data for waters from six estuaries and 15 rivers. The estuarine waters (salinity < 10‰) displayed $(Sm/Yb)_{CN}$ that ranged from 0.63 to 4.74, while $(Sm/Yb)_{CN}$ of the river waters varied between 0.96 and 4.74. Much of the REY load transported by modern rivers is removed in estuaries by the settling of suspended detrital particles, and by the salinity-induced coagulation and settling of colloidal particles rich in the particle reactive REYs (e.g., Sholkovitz, 1994), processes that homogenize the widely varying REY distributions observed in modern rivers to produce the REY pattern typical of modern seawater. Elderfield et al. (1990) deduced that the colloidal fraction carried by many rivers would be enriched in the MREEs (shale-normalized) relative to the light and heavy REYs, similar to patterns observed for the Mozaan IFs sampled from the bottom and top of the sequence (Fig. 2), which represent iron formation deposited under the shallowest sea-level conditions. Studies of the Kalix river in Sweden demonstrated that colloidal particles dominate the transport and export of rare earth elements (Ingri et al., 2000), and these colloids consist of two fractions, one Fe-rich and another C-rich (Andersson et al., 2006). General enrichments in MREEs for Fe-rich organic colloids have been observed in the Hudson and Connecticut rivers (Sholkovitz, 1994), and the presence of MREE-enriched river waters has also been documented by Sholkovitz and Szymczak (2000) and Hannigan and Sholkovitz (2001). The speculation that riverine-derived colloidal particles enriched in the MREEs could exert a strong influence on REY distributions in the Mozaan IFs relies on similar processes controlling REY distributions in

Fig. 6. Elemental ratio plots for data sets presented in Fig. 5, with two-component conservative mixing lines for Eu/Sm, Sm/Yb, and Y/Ho (symbols for all plots defined in c): (a) Y/Ho versus Eu/Sm, showing that a 0.1% high-*T* hydrothermal (>350 °C, Bau and Dulski, 1999) fluid contribution to waters with shallow (<500 m) seawater REY distributions (Alibo and Nozaki, 1999) is sufficient to explain Eu/Sm ratios in the Mozaan and Kuruman IFs, (b) Y/Ho versus Sm/Yb, indicating that a significantly higher contribution of hydrothermal fluid (1–5%) may account for these elemental ratios in the Mozaan IFs, and (c) Sm/Yb as a function of Eu/Sm, demonstrating that relatively small (0.1%) contributions of black smoker fluid can model Sm/Yb and Eu/Sm behavior in the Kuruman and Isua IFs, but do not adequately account for the relative distribution of these elements in the Mozaan IFs.

both modern and Archean rivers and estuaries. However, such processes have not yet been supported by strong evidence from the geologic record, and thus the Mozaan IFs are a first hint at their presence in the Archean.

5.3. Sources of Nd to Archean seawater

5.3.1. Nd in Archean iron formations

To further constrain solute sources supplying the margin of the Kaapvaal craton 2.9 Ga, three of the shale samples and seven of the iron-formation samples were selected for Nd isotopic analyses (Table 3). Neodymium isotopic variations in Archean IFs have been examined by previous workers in attempts to distinguish the source of REY and Fe in these sediments. Miller and O'Nions (1985) concluded that continental Nd dominated the isotopic signature of Precambrian IFs. Jacobsen and Pimentel-Klose (1988a) discussed the likelihood that Archean surface seawater displayed continental signatures derived from fluvial inputs, but concluded that these inputs were an insignificant source of Nd and Fe to Archean IFs and that both Nd and Fe were almost exclusively sourced from a hydrothermal component similar to the flux emanating from modern mid-ocean ridges. Subsequent studies also suggested REY in Archean IFs were derived from sources with depleted-mantle Nd isotopic ratios (Shimizu et al., 1990), and Alibert and McCulloch (1993) proposed that ~50% of Nd in 2.5 Ga Hamersley IFs was derived from Archean mid-ocean ridge sources with $\epsilon_{Nd}(t) = +4$. A similar conclusion was drawn for the 2.5 Ga Kuruman and Penge IFs deposited on the Kaapvaal craton (Bau et al., 1997).

Neodymium isotopic data for Precambrian IFs vary, with samples generally possessing $\epsilon_{Nd}(t)$ between −5 and +5 (Fig. 7). Therefore, it seems likely that the seawater from which these IFs precipitated possessed variable ϵ_{Nd} values, and that Archean–Paleoproterozoic oceans commonly ranged within ±5 $\epsilon_{Nd}(t)$-units relative to CHUR. The IF samples from this study exhibit ϵ_{Nd}(2.9 Ga) values that range over 9 ϵ-units, and the Nd isotope ratios observed in the Mozaan IFs are different from most mid- to late-Archean IFs, which tend towards chondritic or positive $\epsilon_{Nd}(t)$ values. One highly negative $\epsilon_{Nd}(t)$ value of −8.1 for 3.45 Ga iron formation from the Fig Tree/Moodies sequence of the Barberton greenstone belt (BGB) was reported by Miller and O'Nions (1985). This sample (SL 28 B) was a small fragment from an individual magnetite band within the whole-rock sample SL 28 A, which alternatively displayed $\epsilon_{Nd}(t) = +1.1$, similar to $\epsilon_{Nd}(t) = +0.3$ for a second whole-rock sample analysed by these authors. Two additional analyses of Fig Tree Group IF by Jacobsen and Pimentel-Klose (1988b) reported $\epsilon_{Nd}(t)$ of +2.9 and +4.1. If the highly negative value of −8.1 reported by Miller and O'Nions (1985) for sample SL 28 B is atypical of Barberton IF, then these data suggest that IFs deposited prior to 3.0 Ga on or near the Kaapvaal craton would likely display chondritic or slightly positive $\epsilon_{Nd}(t)$. This Nd isotopic behavior is also observed in younger South African IFs, as samples from the 2.5 Ga Kuruman and Penge IFs of the Transvaal Supergroup display a narrow range of ϵ_{Nd}(2.5) between −0.2 and +1.9 (Bau et al., 1997).

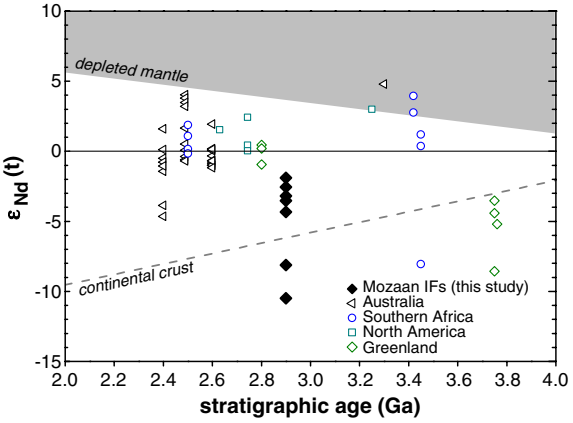

Fig. 7. Initial $\epsilon_{Nd}(t)$ values for Precambrian IFs from literature data. The grey area in the top portion of the figure represents $\epsilon_{Nd}(t)$ values predicted for Nd isotopic evolution in a depleted mantle region with an intial $\epsilon_{Nd}(4.56\ Ga) = 0$ and $\epsilon_{Nd}(0) = +10$, while the dashed line in the lower portion represents a simple continental crust trend for Nd isotopic evolution where $\epsilon_{Nd}(4.56\ Ga) = 0$ and $\epsilon_{Nd}(0) = -17$. In order to facilitate comparison with the present study, data have been screened for samples described as oxide-facies IF by authors, and are from: Miller and O'Nions (1985), Jacobsen and Pimentel-Klose (1988a,b; recalculated using $^{146}Nd/^{144}Nd = 0.7219$), Shimizu et al. (1990), Alibert and McCulloch (1993, 12 Marra Mamba IFs), and Bau et al. (1997). Three analyses of Isua IFs by Shimizu et al. (1990) which display $\epsilon_{Nd}(3.7) > +10$ are not shown. Most Archean oxide facies iron formations that appear to have retained a primary isotopic Nd signature cluster within ±5 ϵ-units of $\epsilon_{Nd}(t) = 0$ (chondritic evolution), with notable exceptions being samples from Isua, and two samples from this study (see text). Nd isotopic data from Frei et al. (1999) for Isua are not included, as they represent additional analyses of sample 242573 which was originally described by Miller and O'Nions (1985). Sample 242573 provided all but one Nd isotope analyses of Isua IFs as reported by Miller and O'Nions (1985) and Frei et al. (1999), and displays $\epsilon_{Nd}(t)$ values that range from −8.6 to +14.8, leading Frei et al. (1999) to suggest that this sample did not retain a primary Nd isotopic signature.

5.3.2. Nd in Mozaan shales

The shale samples are correlated with respect to their Sm–Nd isotope systematics (Fig. 8), and these data suggest that the shales observed relatively closed-system behavior with respect to their Nd isotopic evolution. The shales have model ages (T_{DM}; Jacobsen and Pimentel-Klose, 1988a) of 3.4 ± 0.1 Ga, that agree well with U–Pb SHRIMP dates for individual zircon grains from the siliciclastic Dipka member underlying the IFs, which are predominantly >3.2 Ga as reported by Nhleko (2003). However, previous Nd isotope studies of Mozaan Group fine-grained clastic sediments have revealed a wide range of T_{DM} ages of 1.52–4.73 Ga (Dia et al., 1990) and 2.92–4.63 Ga (Jahn and Condie, 1995), leading Jahn and Condie (1995) to surmise that Pongola pelites had very diverse provenances or that some samples were affected by open-system behavior during diagenesis or low-grade metamorphism. This large range in Sm–Nd isotopic data was not observed, however, by Stevenson and Patchett (1990), who sampled three Mozaan shales from a single locality and reported $\epsilon_{Nd}(t)$ values be-

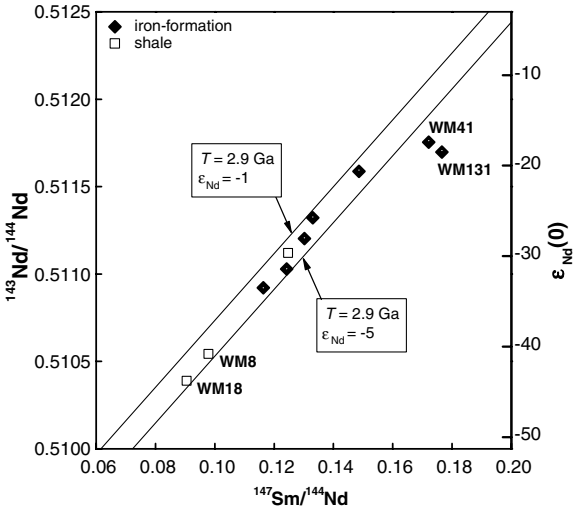

Fig. 8. Analytical results for Nd isotope analyses of Mozaan shales and iron-formation samples, including $\epsilon_{Nd}(0)$ values. Reference isochrons for $\epsilon_{Nd}(t)$ of -1 and -5 bracket all samples from this study, except for IF samples WM41 and WM131. The similarity in the Nd isotopic evolution for the majority of the IFs and the three shale samples suggests that REY sources for the shallow seawater which precipitated the Mozaan IFs were predominately derived from continental crust low in radiogenic Nd.

tween -1.9 to -0.9 (Fig. 8). This suggests that high-resolution sampling (as in this study) of Mozaan fine-grained clastic sediment provides consistent Nd isotopic data supporting relatively homogeneous provenances over short geologic time spans.

Sample WM8 exhibits a similar Si concentration compared to the other three Mozaan shales, but has a much higher Fe content (29% compared to 6–10%, respectively), and a correspondingly lower Al content. Since this aluminous Fe-rich sample resides between two IF bands, it is possible that its major element composition reflects dilution with IF-type precipitates, and the Fe increase occurred at the expense of aluminium-rich phases. Samples WM8 and WM18 have Sm and Nd concentrations that differ by more than a factor of six, yet display very similar $^{147}Sm/^{144}Nd$ and $^{143}Nd/^{144}Nd$.

5.3.3. Nd in Mozaan iron formations

The good agreement in Sm–Nd isotope systematics between the shales and the majority of the IF samples (Fig. 8) argues against a significant REY component derived from a depleted mantle source contributing to local seawater. However, the IF samples do display the positive shale-normalized Eu anomalies typical of Archean IFs, which requires some high-T hydrothermal REY input. It appears that such a high-T input, however, did not overwhelm the terrestrial flux in terms of the Nd isotope signature. The relationship between Eu anomalies and Sm–Nd isotopic signatures in Archean iron-formations was examined by Derry and Jacobsen (1990), who considered two-component conservative mixing between East Pacific Rise hydrothermal fluids and estimated river water. These authors concluded that Eu fractionation due to scavenging of Eu^{2+} near vent sites renders these anomalies unsuitable for mass balance calculations in IFs and that more reliable mass fraction estimates are obtained using the Nd isotopic mass balance. However, the inability to reconcile Nd and Eu mass balance calculations from the mixing of hydrothermal and river/seawater endmembers is expected, as only the Nd isotopic signature provides information regarding the relative mass fractions of the REY sources; Eu anomalies only provide information regarding the temperature of REY sources. An extreme example of the lack of correlation between mantle-like Nd isotopic signatures and positive Eu anomalies in high-T marine hydrothermal fluids (and hence, IFs) may be found in the data of Piepgras and Wasserburg (1985). These authors reported Nd isotopic data for a hydrothermal system developed on a sediment covered ridge in the Guaymas Basin. This system vented hydrothermal fluid in excess of 300 °C, which migrated through a sedimentary package several hundred meters thick and possessed a positive Eu anomaly coupled with $\epsilon_{Nd}(0) = -11.4$, indicating that marine fluids hot enough to fractionate Eu from other REY will display Nd isotopic signatures similar to the host rock (in this case, continentally-derived sediments). This illustrates that positive Eu anomalies cannot be used to constrain MORB-derived hydrothermal inputs, as they provide little information regarding the source of REYs to high-T fluids, but rather reflect only the temperature of the hydrothermal system.

Of the seven IF samples, five appear to have experienced an Nd isotopic evolution similar to that of the shales, consistent with these samples (both shales and IFs) having received Nd from an isotopically similar source. Two of the Pongola IF samples, WM41 and WM131, are not consistent with a single isotopic source or closed-system conditions following deposition. These samples differ primarily in their high $^{147}Sm/^{144}Nd$ (>0.17), compared to a $^{147}Sm/^{144}Nd$ average of 0.13 ± 0.01 for the remaining five IFs. Considering that WM41 and WM131 represent the first and last IF beds deposited, respectively, it is unlikely that post-depositional processes (e.g., metamorphism) would selectively affect only these samples. The $^{147}Sm/^{144}Nd$ average of 0.13 ± 0.01 for five of the seven Mozaan IFs is identical to the average obtained (0.13 ± 0.03) from a survey of 61 analyses of predominantly oxide facies Archean and Paleoproterozoic IFs (Miller and O'Nions, 1985; Jacobsen and Pimentel-Klose, 1988a,b; Shimizu et al., 1990; Alibert and McCulloch, 1993; Bau et al., 1997). Of these literature data, only three samples (two from the Hamersley Basin and one Barberton greenstone belt sample) have higher $^{147}Sm/^{144}Nd$ than samples WM31 and WM141. Alibert and McCulloch (1993) reported data for 26 samples from the Dales Gorge and Joffre IFs, concluding on the basis of Nd isotopes that these IFs had suffered a metamorphic resetting of their isotopic system some 500 Ma after deposition, a conclusion supported by Rb–Sr and Pb–Pb isotopic analyses of the underlying Fortescue lavas (Nelson et al., 1992). The $^{147}Sm/^{144}Nd$ of these 26 metamorphosed IF samples averages 0.12 ± 0.02. It therefore seems that metamorphic events in Archean IFs capable of altering Nd isotope ratios have little effect

on overall $^{147}Sm/^{144}Nd$ values, an observation that supports the view of Bau (1993), who concluded that REY exhibited little mobility during all but the most severe grades of metamorphism. This suggests that the high $^{147}Sm/^{144}Nd$ observed in samples WM41 and WM131 is primary in origin. If these samples represent closed-system behavior, as the other IF and shale samples appear to, then they require a source with a lower initial $^{143}Nd/^{144}Nd$ (characteristic of continental crust), coupled with a Sm/Nd ratio typical of more mafic sources, and as such, they remain ambiguous.

The IF samples that closely follow the Nd systematics of the shales display the two distinct types of REY distributions discussed earlier. WM51 and WM61 exhibit the MREE to HREE depleted patterns typical at the onset of IF deposition, whereas the remaining three samples possess REY patterns that are relatively flat from the MREE to HREE. The isotopic similarity between the IFs and shales suggests that soluble REY delivered to the iron-formation originated from contemporaneous continental crust. The least radiogenic shale sample displays $\epsilon_{Nd}(2.9\ Ga) = -4.2$, so it is reasonable that local continental crust possessed a similar $\epsilon_{Nd}(2.9\ Ga)$ value. Assuming the mid-ocean ridge hydrothermal flux displayed $\epsilon_{Nd}(2.9\ Ga) = +4$, and assigning the continental flux an $\epsilon_{Nd}(2.9\ Ga)$ value of -4.2, then Nd isotopic mass balance calculations require that between 72% and 100% of the Nd in these IF samples ($\epsilon_{Nd}(2.9\ Ga)$ of -1.9 to -4.3) must have originated from a source(s) possessing an Nd isotopic signature similar to local continental crust. If this was the case, this source should possess a REY distribution similar to that of the Mozaan shale average WMS, and deviations from the WMS pattern within a pure chemical sediment would originate from processes occurring solely within the water column (i.e., chemical complexation and scavenging on Fe-oxyhydroxide particles, etc.). The geologic evidence for a transgressive–regressive cycle of deposition, coupled with the evolution of the REY patterns in the Mozaan IFs with stratigraphic position, suggests that varying proportions of a continentally-derived solute source dominated trace element evolution in shallow seawater near the Kaapvaal craton ~3.0 Ga ago. Therefore, it is possible that the MREE-enriched patterns observed in modern low salinity coastal seas and estuaries (Elderfield et al., 1990) represent processes analogous to those that controlled the REY distributions observed in the Mozaan IFs. Unlike modern environments, the importance of organic compounds and organic-based colloidal particles on REY distributions in Archean marine settings is difficult to estimate, though the presence of stromatolitic carbonate in the underlying Nsuze Group (Mason and von Brunn, 1977; Beukes and Lowe, 1989) indicates that the margin of the Kaapvaal craton was colonized by microbial communities prior to deposition of the Mozaan IFs. It is therefore not unreasonable to expect that organic constituents exerted some effect on local geochemical processes, and the above observations are consistent with non-redox sensitive processes similar to modern ones operating in shallow seas on Archean continental margins.

The negative $\epsilon_{Nd}(2.9\ Ga)$ values for the Mozaan IFs are not entirely unusual, however, as supported by negative $\epsilon_{Nd}(t)$ values for some younger IFs, as well as by recent investigations of Archean shallow water carbonates from southern Africa (Bolhar et al., 2002; Kamber et al., 2004). These studies concluded that near-shore seawater displayed REY and Nd isotope signatures indicative of local solute inputs derived from continental weathering, and offer further support suggesting that shallow seawater during the mid- to late-Archean was strongly influenced by continentally-derived solute fluxes.

A final comment regarding the correlation between Sm–Nd isotope ratios and Fe in Archean IFs is warranted. Previous workers have calculated the mass fraction of Fe derived from different sources by conservatively mixing a hydrothermal endmember possessing a depleted-mantle Nd isotope ratio with a river/seawater endmember which possesses a continental Nd isotope signature (e.g., Miller and O'Nions, 1985; Jacobsen and Pimentel-Klose, 1988a). While conclusions have varied regarding the dominant Fe source, these attempts have all relied on assumptions regarding the Fe/Nd ratio of the endmembers, and crucial to the models is the requirement that Fe/Nd did not change significantly in the Archean ocean. However, there existed processes in the Archean ocean, such as pyrite precipitation close to hydrothermal vent sites, and IF precipitation itself, for example, that fractionated Fe and Nd. Moreover, Fe and Nd behavior in the continentally-derived flux produces even more ambiguity due to uncertainties in various parameters such as the pH of river water, local redox conditions, and possible involvement of biological processes. As a result, the current state of knowledge precludes definitive statements regarding the Fe source to Archean IFs based upon Nd isotope systematics.

6. CONCLUSIONS

All of the Mozaan iron-formation samples exhibit major and trace element characteristics typical of very pure marine chemical sediments, including shale-normalized positive La, Gd, and Y anomalies, which are fully consistent with a marine depositional setting. Positive Eu anomalies in all IF samples indicate a high-T hydrothermal source supplied REYs to the seawater which precipitated the Mozaan IFs. The magnitude of this anomaly is consistent with the general trend of decreasing Eu/Eu^* with decreasing age for Precambrian IFs and is within the range for other Archean IFs, though it cannot be used to quantify the magnitude of the high-T hydrothermal flux. The lack of Ce anomalies in all of the IF samples indicates that local, shallow Archean seawater was too reducing to permit oxidation of Ce(III) to Ce(IV), implying relatively low redox levels in the Archean atmosphere compared to present values.

When compared to many other Archean IFs, the Pongola samples have higher Sm/Yb ratios and appear to record a systematic variation in water depth on the margin of the Kaapvaal craton during IF sedimentation. Dominant factors influencing the REY distribution of coastal seawater in the Archean would include atmospheric composition (e.g., ρCO_2) and fluxes of solutes from terrestrial sources. Isotope systematics of Sm–Nd reveal similarity between iron-formation and contemporaneous shale, arguing against an Arche-

an mid-ocean ridge hydrothermal system as the dominant REY source for these IFs. Rare earth elements in both shale and IFs appear to be derived primarily from a relatively homogenous cratonic source older than 3.2 Ga, and consistent Nd isotopic behavior can be observed in Pongola sediments that sample relatively short geologic time spans. These data imply that solutes within shallow seawater along Archean cratonic margins were sourced primarily from weathering of continental crust. The Nd isotopic data for the Mozaan shales (T_{DM} of 3.4 ± 0.1 Ga) and the depositional age of these sediments suggests that local continental crust was stable on 100 Ma time-scales, and when coupled with the laterally extensive nature of the precipitated Mozaan IFs, this implies that by 2.9 Ga ago a significant amount of continental crust was exposed to weathering.

ACKNOWLEDGMENTS

We appreciate the assistance of Marina Fischerström and Hans Schöberg with the Sm–Nd isotopic analyses performed at LIG. Furthermore, this manuscript significantly benefited from the comments of A. Bekker and one anonymous reviewer, and their efforts are gratefully acknowledged. We also thank T. Lyons for helpful suggestions and editorial guidance.

REFERENCES

Alibert C. and McCulloch M. T. (1993) Rare earth element and Nd isotopic compositions of the banded iron-formations and associated shales from Hamersley, Western Australia. *Geochim. Cosmochim. Acta* **57**, 187–204.

Alibo D. S. and Nozaki Y. (1999) Rare earth elements in seawater: particle association, shale-normalization, and Ce oxidation. *Geochim. Cosmochim. Acta* **63**, 363–372.

Anders E. and Grevesse N. (1989) Abudances of the elements: meteoric and solar. *Geochim. Cosmochim. Acta* **53**, 197–214.

Andersson K., Dahlqvist R., Turner D., Stolpe B., Larsson T., Ingri J. and Andersson P. (2006) Colloidal rare earth elements in a boreal river: changing sources and distributions during the spring flood. *Geochim. Cosmochim. Acta* **70**, 3261–3274.

Barrett T. J., Fralick P. W. and Jarvis I. (1988) Rare-earth-element geochemistry of some Archean iron formations north of Lake Superior, Ontario. *Can. J. Earth Sci.* **25**, 570–580.

Bau M. (1991) Rare earth element mobility during hydrothermal and metamorphic fluid–rock interaction and the significance of the oxidation state of europium. *Chem. Geol.* **93**, 219–230.

Bau M. (1993) Effects of syn- and post-depositional processes on the rare-earth element distribution in Precambrian iron-formations. *Eur. J. Mineral.* **5**, 257–267.

Bau M. (1999) Scavenging of dissolved yttrium and rare earths by precipitating iron oxyhydroxide: experimental evidence for Ce-oxidation, Y–Ho fractionation, and lanthanide tetrad effect. *Geochim. Cosmochim. Acta* **63**, 67–77.

Bau M. and Dulski P. (1992) Small-scale variations of the rare-earth element distribution in Precambrian iron formations. *Eur. J. Mineral.* **4**, 1429–1433.

Bau M. and Dulski P. (1996) Distribution of yttrium and rare-earth elements in the Penge and Kuruman iron-formations, Transvaal Supergroup, South Africa. *Precamb. Res.* **79**, 37–55.

Bau M. and Dulski P. (1999) Comparing yttrium and rare earths in hydrothermal fluids from the Mid-Atlantic Ridge: implications for Y and REE behaviour during near-vent mixing and for the Y/Ho ratio of Proterozoic seawater. *Chem. Geol.* **155**, 77–90.

Bau M. and Möller P. (1993) Rare earth element systematics of the chemically precipitated component in Early Precambrian iron formations and the evolution of the terrestrial atmosphere–hydrosphere–lithosphere system. *Geochim. Cosmochim. Acta* **57**, 2239–2249.

Bau M., Koschinsky A., Dulski P. and Hein J. R. (1996) Comparison of the partitioning behaviours of yttrium, rare earth elements, and titanium between hydrogenetic marine ferromanganese crusts and seawater. *Geochim. Cosmochim. Acta* **60**, 1709–1725.

Bau M., Höhndorf A., Dulski P. and Beukes N. J. (1997) Sources of rare-earth elements and iron in Paleoproterozoic iron-formations from the Transvaal Supergroup, South Africa: Evidence from neodymium isotopes. *J. Geol.* **105**, 121–129.

Bau M., Usui A., Pracejus B., Mita N., Kanai Y., Irber W. and Dulski P. (1998) Geochemistry of low-temperature water–rock interaction: evidence from natural waters, andesite, and iron-oxyhydroxide precipitates at Nishiki-numa iron-spring, Hokkaido, Japan. *Chem. Geol.* **151**, 293–307.

Beukes N. J. and Cairncross B. (1991) A lithostratigraphic-sedimentological reference profile for the late Archaean Mozaan Group, Pongola Sequence: application to sequence stratigraphy and correlation with the Witwatersrand Supergroup. *S. Afr. J. Geol.* **94**, 44–69.

Beukes N. J. and Lowe D. R. (1989) Environmental control on diverse stromatolite morphologies in the 3000 Myr Pongola Supergroup, South Africa. *Sedimentology* **36**, 383–397.

Bolhar R., Hofmann A., Woodhead J., Hergt J. and Dirks P. (2002) Pb- and Nd-isotope systematics of stromatolitic limestones from the 2.7 Ga Ngezi Group of the Belingwe Greenstone Belt: constraints on timing of deposition and provenance. *Precamb. Res.* **114**, 277–294.

Bolhar R., Kamber B. S., Moorbath S., Fedo C. M. and Whitehouse M. J. (2004) Characterisation of early Archaean chemical sediments by trace element signatures. *Earth Planet. Sci. Lett.* **222**, 43–60.

Button A., Pretorius D. A., Jansen H., Stocklmayer V., Hunter D. R., Wilson J. F., Wilson A. H., Vermaak C. A., Lee C. A. and Stagman J. G. (1981) The cratonic environment: the Pongola Supergroup. In *Precambrian of the Southern Hemisphere* (ed. D. R. Hunter). Elsevier Scientific Publications Co., Amsterdam, pp. 501–510.

Danielson A., Möller P. and Dulski P. (1992) The europium anomalies in banded iron formations and the thermal history of the oceanic crust. *Chem. Geol.* **97**, 89–100.

DePaolo D. J. and Wasserburg G. J. (1976) Nd isotopic variations and petrogenetic models. *Geophys. Res. Lett.* **3**, 249–252.

Derry L. A. and Jacobsen S. B. (1990) The chemical evolution of Precambrian seawater: evidence from rare earth elements in banded iron formations. *Geochim. Cosmochim. Acta* **54**, 2965–2977.

Dia A., Allègre C. J. and Erlank A. J. (1990) The development of continental crust through geological time: the South African case. *Earth Planet. Sci. Lett.* **98**, 74–89.

Dulski P. (2001) Reference materials for geochemical studies: new analytical data by ICP-MS and critical discussion of reference values. *Geostand. Newslett.* **25**, 87–125.

Elderfield H. (1988) The oceanic chemistry of the rare-earth elements. *Phil. Trans. R. Soc. London Ser. A* **325**, 105–126.

Elderfield H., Upstill-Goddard R. and Sholkovitz E. R. (1990) The rare earth elements in rivers, estuaries, and coastal seas and their significance to the composition of ocean waters. *Geochim. Cosmochim. Acta* **54**, 971–991.

Erel Y. and Stolper E. M. (1993) Modeling of rare-earth element partitioning between particles and solution in aquatic environments. *Geochim. Cosmochim. Acta* **57**, 513–518.

Frei R., Bridgewater D., Rosing M. and Stecher O. (1999) Controversial Pb–Pb and Sm–Nd isotope results in the early Archean Isua (West Greenland) oxide iron formation: preservation of primary signatures versus secondary disturbances. *Geochim. Cosmochim. Acta* **63**, 473–488.

Fryer B. J. (1977) Rare earth evidence in iron formations for changing Precambrian oxidation states. *Geochim. Cosmochim. Acta* **41**, 361–367.

Grauch R. I. (1989) Rare earth elements in metamorphic rocks. In *Geochemistry and Mineralogy of Rare Earth Elements* (eds. B. R. Lipin and G. A. McKay); *Rev. Mineral.* **21**, 147–167, Mineral. Soc. Amer.

Gross G. A. (1983) Tectonic systems and the deposition of iron-formation. *Precamb. Res.* **20**, 171–187.

Hannigan R. E. and Sholkovitz E. R. (2001) The development of middle rare earth element enrichments in freshwaters: weathering of phosphate minerals. *Chem. Geol.* **175**, 495–508.

Hegner E., Kröner A. and Hofmann A. W. (1984) Age and isotope geochemistry of the Archaean Pongola and Usushwana suites in Swaziland, southern Africa: a case for crustal contamination of mantle-derived magma. *Earth Planet. Sci. Lett.* **70**, 267–279.

Hunter D. R. and Wilson A. H. (1988) A continuous record of Archaean evolution from 3.5 Ga to 2.6 Ga in Swaziland and northern Natal. *S. Afr. J. Geol.* **91**, 57–74.

Ingri J., Widerlund A., Land M., Gustafsson O., Andersson P. and Ohlander B. (2000) Temporal variations in the fractionation of the rare earth elements in a boreal river; the role of colloidal particles. *Chem. Geol.* **166**, 23–45.

Jacobsen S. B. and Pimentel-Klose M. R. (1988a) A Nd isotopic study of the Hammersley and Michipicoten banded iron formations: The source of REE and Fe in Archean oceans. *Earth Planet. Sci. Lett.* **87**, 29–44.

Jacobsen S. B. and Pimentel-Klose M. R. (1988b) Nd isotopic variations in Precambrian banded iron formations. *Geophys. Res. Lett.* **15**, 393–396.

Jahn B. and Condie K. C. (1995) Evolution of the Kaapvaal Craton as viewed from geochemical and Sm–Nd isotopic analyses of intracratonic pelites. *Geochim. Cosmochim. Acta* **59**, 2239–2258.

James H. L. and Trendall A. F. (1982) Banded iron formation: distribution in time and paleoenvironmental significance. In *Mineral Deposits and Evolution of the Biosphere* (eds. H. D. Holland and M. Schidlowski). Springer, Berlin, pp. 199–217.

Kamber B. S. and Webb G. E. (2001) The geochemistry of late Archaean microbial carbonate: Implications for ocean chemistry and continental erosion history. *Geochim. Cosmochim. Acta* **65**, 2509–2525.

Kamber B. S., Bohlar R. and Webb G. E. (2004) Geochemistry of late Archaean stromatolites from Zimbabwe: evidence for microbial life in restricted epicontinental seas. *Precamb. Res.* **132**, 379–399.

Kato Y., Ohta I., Tsunematsu T., Watanabe Y., Isozaki Y., Maruyama S. and Imai N. (1998) Rare earth element variations in mid-Archean banded iron formations: implications for the chemistry of ocean and continent and plate tectonics. *Geochim. Cosmochim. Acta* **62**, 3475–3497.

Khan R. M. K., Das Sharma S., Patil D. J. and Naqvi S. M. (1996) Trace, rare-earth element, and oxygen isotopic systematics for the genesis of banded iron-formations: evidence from the Kushtagi schist belt, Archaean Dharwar Craton, India. *Geochim. Cosmochim. Acta* **60**, 3285–3294.

Klein C. and Beukes N. J. (1989) Geochemistry and sedimentology of a facies transition from limestone to iron-formation deposition in the Early Proterozoic Transvaal Supergroup, South Africa. *Econ. Geol.* **84**, 1733–1774.

Klemm D. D. (2000) The formation of Palaeoproterozoic banded iron formations and their associated Fe and Mn deposits, with reference to the Griqualand West deposits, South Africa. *J. Afr. Earth Sci.* **30**, 1–24.

Kulaksiz S. and Bau M. (2007) Contrasting behaviour of anthropogenic gadolinium and natural rare earth elements in estuaries and the gadolinium input into the North Sea. *Earth Planet. Sci. Lett.* **260**, 361–371.

Mason T. R. and von Brunn V. (1977) 3-Gyr-old stromatolites from South Africa. *Nature* **266**, 47–49.

Matthews P. E. (1967) The pre-Karroo formations of the White Umfolozi inlier, northern Natal. *Trans. Geol. Soc. S. Afr.* **70**, 39–63.

McLennan S. M. (1989) Rare earth elements in sedimentary rocks: influence of provenance and sedimentary processes. In *Geochemistry and Mineralogy of Rare Earth Elements* (eds. B.R. Lipin and G.A. McKay); *Rev. Mineral.* 21, 169–200, Mineral. Soc. Amer.

McLennan S. M., Taylor S. R. and Kröner A. (1983) Geochemical evolution of Archean shales from South Africa. I. The Swaziland and Pongola Supergroups. *Precamb. Res.* **22**, 93–124.

Michard A. (1989) Rare earth element systematics in hydrothermal fluids. *Geochim. Cosmochim. Acta* **53**, 745–750.

Miller R. G. and O'Nions R. K. (1985) Sources of Precambrian chemical and clastic sediments. *Nature* **314**, 325–330.

Morris R. C. (1993) Genetic moelling for banded iron-formation of the Hamersley Group, Pilbara Craton, Western Australia. *Precamb. Res.* **60**, 243–286.

Nelson D. R., Trendall A. F., de Laeter J. R., Grobler N. J. and Fletcher I. R. (1992) A comparative study of the geochemical and isotopic systematics of late Archean flood basalts from the Pilbara and Kaapvaal cratons. *Precamb. Res.* **54**, 231–256.

Nhleko N. (2003) The Pongola Supergroup in Swaziland, Ph.D. dissertation Rand Afrikaans University.

Nothdurft L. D., Webb G. E. and Kamber B. S. (2004) Rare earth element geochemistry of Late Devonian reefal carbonates, Canning Basin, Western Australia: confirmation of a seawater REE proxy in ancient limestones. *Geochim. Cosmochim. Acta* **68**, 263–283.

Pichler T., Veizer J. and Hall G. E. M. (1999) The chemical composition of shallow-water hydrothermal fluids in Tutum Bay, Ambitle Island, Papua New Guinea and their effect on ambient seawater. *Mar. Chem.* **64**, 229–252.

Piepgras D. J. and Wasserburg G. J. (1980) Neodymium isotopic variations in seawater. *Earth Planet. Sci. Lett.* **50**, 128–138.

Piepgras D. J. and Wasserburg G. J. (1985) Strontium and neodymium isotopes in hot springs on the East Pacific rise and Guaymas basin. *Earth Planet. Sci. Lett.* **72**, 341–356.

Shields G. and Stille P. (2001) Diagenetic constraints on the use of cerium anomalies as palaeoseawater redox proxies: an isotopic and REE study of Cambrian phosphorites. *Chem. Geol.* **175**, 29–48.

Shields G. A. and Webb G. E. (2004) Has the REE composition of seawater changed over geological time? *Chem. Geol.* **204**, 103–107.

Shimizu H., Umemoto N., Masuda A. and Appel P. W. U. (1990) Sources of iron-formations in the Archean Isua and Malene supracrustals, West Greenland: evidence from La–Ce and Sm–Nd isotopic data and REE. *Geochim. Cosmochim. Acta* **54**, 1147–1154.

Sholkovitz E. R. (1994) The aquatic chemistry of rare earth elements in rivers and estuaries. *Aqua. Geochem.* **1**, 3–34.

Sholkovitz E. and Szymczak R. (2000) The estuarine chemistry of rare earth elements: comparison of the Amazon, Fly, Sepik and the Gulf of Papua systems. *Earth Planet. Sci. Lett.* **179**, 299–309.

Stevenson R. K. and Patchett P. J. (1990) Implications for the evolution of continental crust from Hf isotope systematics of Archean detrital zircons. *Geochim. Cosmochim. Acta* **54**, 1683–1697.

Tankard A. J., Jackson M. P. A., Eriksson K. A., Hobday D. K., Hunter D. R. and Minter W. E. L. (1982) *Crustal Evolution of Southern Africa*. Springer Verlag, New York.

Taylor S. R. and McLennan S. M. (1985) *The continental crust: its composition and evolution*. Blackwell Scientific, Oxford.

Towe K. M. (1991) Aerobic carbon cycling and cerium oxidation: significance for Archean oxygen levels and banded iron-formation deposition. *Palaeogeo. Palaeoclim. Palaeoecol.* **97**, 113–123.

von Brunn V. and Hobday D. K. (1976) Early Precambrian tidal sedimentation in the Pongola Supergroup of South Africa. *J. Sediment. Petrol.* **46**, 670–679.

von Brunn V. and Mason T. R. (1977) Siliciclastic-carbonate tidal deposits from the 3000 M.Y. Pongola Supergroup, South Africa. *Sediment. Geol.* **18**, 245–255.

Watchorn M. B. (1980) Fluvial and tidal sedimentation in the 3000 Ma Mozaan basin, South Africa. *Precamb. Res.* **13**, 27–42.

Webb G. E. and Kamber B. S. (2000) Rare earth elements in Holocene reefal microbialites: a new shallow seawater proxy. *Geochim. Cosmochim. Acta* **64**, 1557–1565.

Weilers B. F. (1990) A review of the Pongola Supergroup and its setting on the Kaapvaal craton. Econ. Geol. Res. Unit, Info. Cir. No. 228, Univ. Witwatersrand.

Wheat C. G., Mottl M. J. and Rudnicki M. (2002) Trace element and REE composition of a low-*T*emperature ridge-flank hydrothermal spring. *Geochim. Cosmochim. Acta* **66**, 3693–3705.

Wronkiewicz, D. J. (1989) Geochemistry and mineralogy of mid-Archean to mid-Proterozoic sediments from the Kaapvaal craton, southern Africa: source area provenance, weathering tectonic setting and crustal evolution. Ph.D. dissertation New Mexico Inst. Mining Tech.

Associate editor: Timothy W. Lyons